Available online at www.sciencedirect.com
ScienceDirect
Journal of Bionic Engineering 12 (2015) 643–655

DTM Simulation of Peristaltic Viscoelastic Biofluid Flow in Asymmetric Porous Media: A Digestive Transport Model

Dharmendra Tripathi[1], Osman Anwar Bég[2], Praveen Kumar Gupta[3], Ganjam Radhakrishnamacharya[4], Jagannath Mazumdar[5]

1. *Department of Mechanical Engineering*, *Manipal University Jaipur*, *Jaipur* 303007, *India*
2. *Gort Engovation-Bio-Propulsion Research*, *Gabriel's Wing House*, *Bradford* BD6 1FA, *UK*
3. *Department of Mathematics*, *National Institute of Technology Silchar, Silchar* 788010, *India*
4. *Department of Mathematics*, *National Institute of Technology*, *Warangal* 506004, *India*
5. *School of Electrical & Electronic Engineering*, *The University of Adelaide*, *Adelaide* SA 5005, *Australia*

Abstract

A biofluid dynamics mathematical model is developed to study peristaltic flow of non-Newtonian physiological liquid in a two-dimensional asymmetric channel containing porous media as a simulation of obstructed digestive (intestinal) transport. The fractional Oldroyd-B viscoelastic rheological model is utilized. The biophysical flow regime is constructed as a wave-like motion and porous medium is simulated with a modified Darcy-Brinkman model. This model is aimed at describing the digestive transport in intestinal tract containing deposits which induce impedance. A low Reynolds number approximation is employed to eliminate inertial effects and the wavelength to diameter ratio is assumed to be large. The differential transform method (DTM), a semi-computational technique is employed to obtain approximate analytical solutions to the boundary value problem. The influences of fractional (rheological material) parameters, relaxation time, retardation time, amplitude of the wave, and permeability parameter on peristaltic flow characteristics such as volumetric flow rate, pressure difference and wall friction force are computed. The present model is relevant to flow in diseased intestines.

Keywords: peristaltic transport, fractional Oldroyd-B model, porous medium, differential transform method, asymmetric channel, obstructed digestive flow

doi: 10.1016/S1672-6529(14)60154-2

Nomenclature

h_1	Transverse vibration of the upper wall
h_2	Transverse vibration of the lower wall
b_1	Upper half-width of the channel
b_2	Lower half-width of the channel
a_1	Amplitude of upper wall
a_2	Amplitude of lower wall
ξ	Axial displacement
u	Axial velocity
v	Transverse velocity
η	Transverse coordinate
p	Pressure
Re	Reynolds number
c	Wave velocity
K	Permeability parameter
q	Volumetric flow rate in the wave frame
δ	Wave number
ϕ_1	Ratio of upper wall wave amplitude to upper channel half width
ϕ_2	Ratio of lower wall wave amplitude to upper channel half width
ϕ	Phase difference
μ	Viscosity
α, β	Fractional parameters
ψ	Stream function
φ	Porosity of porous medium
λ	Wavelength
$\tilde{\tau}$, $\dot{\gamma}$	Shear stress, rate of shear strain
$\overline{\lambda}_1$, $\overline{\lambda}_2$	Material constants
ρ	Fluid density

Corresponding author: Dharmendra Tripathi
E-mail: dharmtri@gmail.com

1 Introduction

The muscular layers of the digestive tract comprise smooth muscle tissue, which triggers peristaltic and segmentation movements. Peristalsis propels a small mass of digestive contents called a bolus along the length of digestive tract. In intestines, over a period of time, digestive deposits may harden and cause obstructions. In severe cases, such as acute distention of the bowel, serious ailments may result, where normal transport is dangerously impeded. Numerous gastroenterological medical researchers have investigated a range of such phenomena including Elman[1], Grassi *et al*.[2] (who employed sonography), Farrel[3], Rommel *et al*.[4] and Kishi *et al*.[5], the latter examining specifically Bouveret's syndrome. It has been suggested in recent studies that mathematical models of flows in obstructed systems may be mimicked using a porous media hydrodynamics approach. Indeed there are a large number of simulation techniques available in the literature which may be aimed at analysing impedance effects of various models, such as Darcy models, Darcy-Brinkman models, Darcy-Forchheimer models[6], and tortuosity models[7]. These techniques may employ randomised Sierspinski carpet approaches, multi-scale effects[8], poroelasticity[9] and spatially periodic effects[10]. In the context of peristaltic propulsion in porous media, several studies have been communicated. Kothandapani and Srinivas[11] investigated analytically peristaltic flow in an inclined asymmetric channel containing a porous medium, describing porous media drag effects on trapping for sinusoidal, triangular, square and trapezoidal waveforms. Mekheimer and Abd Elmaboud[12] studied the peristaltic flow in an annular porous regime, as a model of an endoscope, observing that pressure rise has an inverse nonlinear relationship with permeability and that bolus magnitude increases with permeability. El Shehawey and Husseny[13] obtained perturbation solutions for peristaltic pumping by a sinusoidal traveling wave in a porous medium channel with wall suction. They found that the mean axial velocity and backflow increase with greater permeability parameter and that fluid motion is non-symmetric. Further studies were communicated by Mekheimer[14] for inclined channels and Srinivas and Gayathri[15] for heat transfer effects. These models[11–15] considered the transport fluid to be Newtonian and essentially creeping flow approximations of the Navier-Stokes equations with moving boundaries. The rheological nature of digestive fluids including chyme has been established for many decades, and is elaborated among other physiological fluids by Skalak *et al*.[16]. A number of models have therefore emerged to analyse the peristaltic flows of non-Newtonian fluids with a diverse array of constitutive models. These included Ostwald-de Waele pseudoplastic/dilatant models for duodenal flows[17], Carreau models[18] for bile flows, couple stress models for chime transport in small intestines[19], and micropolar models[20]. Another aspect of biorheology is viscoelasticity[21] which features in the dynamics of many gastric fluids, blood, synovial fluid, *etc*. A reduced viscosity is known to be associated with a drop in tensile stresses in a viscoelastic fluid with progression in time, which aids relaxation of the liquid and contributes to a decrease in bulk viscosity of the fluid, as elaborated by Norouzi *et al*.[22]. Recent studies of viscoelastic peristaltic flow include Tripathi[23] who considered generalized Oldroyd-B fluids, Yasmin *et al*.[24] who employed the Johnson-Segalman model, Tripathi *et al*.[25] who utilized the Jeffrey model for oesophagus and Tripathi *et al*.[26] who considered slip flows with generalized Oldroyd-B fluids. These articles however ignored porous media aspects. Recently, several attempts to model non-Newtonian peristaltic flows in porous media have been made. These include Alemayehu and Radhakrishnamacharya[27] who considered hydrodynamic dispersion in micropolar peristaltic flow in a permeable medium and Mekheimer[28] who used the Reiner-Rivlin second order diff erential model for peristaltic rheological flow in a porous conduit. Tripathi and Bég[29] studied transient peristaltic flow of generalized Maxwell fluids through a porous medium, presenting solutions with the homotopy perturbation method. They showed that the size of the trapped bolus is weakly elevated with greater permeability of the porous medium, but diminished with increasing wave amplitude ratio. This study also noted that relaxation time of the viscoelastic fluid has a different influence on different pumping regions of the flow. Further studies addressing non-Newtonian peristaltic porous media hemodynamics include Alemayehu and Radhakrishnamacharya[30] and Tripathi[31] (employing couple stress fluids).

In computational viscoelasticity, a popular trend in recent years has been the fractional derivative model of viscoelastic fluids. This generally entails a classical

differential equation which is modified by replacing the time derivative of an integer order with the so-called Riemann-Liouville fractional calculus operator. This generalization allows one to define precisely non-integer order integrals or derivatives. Oldroyd[32] developed a viscoelastic model to study rheological behavior of materials. This model may also be generalized in the form of a fractional Oldroyd model using fractional calculus. In view of the relevance of fractional models of viscoelastic fluids, a number of authors[33–35] have investigated flow behavior of viscoelastic fluids with fractional Oldroyd-B model, through different geometries and with various wall surface conditions. In these investigations, closed-form solutions for the velocity field and the associated shear stress have been presented using mathematical transforms e.g. Laplace, Fourier, Weber, Hankel, *etc.* Many computational and semi-computational approaches also are available for solving nonlinear boundary value problems in peristaltic biorheology. One example is the Differential Transform Method (DTM) which was first proposed by Zhou[36] to solve linear and non-linear initial value problem in electric circuit analysis. This approach provides excellent versatility and enhanced accuracy[37] in accommodating differential equation systems and also achieved accelerated computation times compared with other methods. In the present study, the DTM is implemented to obtain more accurate solutions for non-Newtonian fractional viscoelastic Oldroyd-B flow in an asymmetric channel containing porous media. Mathematical software is used to obtain graphical solutions for the influence of the geometric and rheological parameters. The current work is relevant to simulation of obstructed digestive (intestinal) transport[1–5], where the debris in the gastric tract is modelled using a Darcy-Brinkman porous media drag force model, valid for low Reynolds number (viscous-dominated) transport.

2 Mathematical model

2.1 Geometric model for peristaltic flow channel

The two-dimensional non-Newtonian biofluid peristaltic flow in an infinite asymmetric channel having width b_1+b_2 is considered which is shown in Fig. 1.An asymmetric flow regime is produced by choosing the peristaltic wave train, travelling with velocity c along the walls to have different amplitudes (a_1, a_2) and phase (ϕ). This amounts to a 'moving boundary' problem. The upper and lower walls of the asymmetric channel (see Fig. 1) are respectively modelled using the relations.

$$\left.\begin{aligned}\tilde{h}_1 &= b_1 + a_1 \sin\left(\frac{2\pi}{\lambda}(\tilde{\xi} - c\tilde{t})\right)\\ \tilde{h}_2 &= -b_2 - a_2 \sin\left(\frac{2\pi}{\lambda}(\tilde{\xi} - c\tilde{t}) + \varphi\right)\end{aligned}\right\}, \tag{1}$$

where λ, ξ, c, $\tilde{t}$ are the wavelength, axial coordinate, wave velocity and time, respectively. The phase difference ϕ varies in the range $0\le\phi\le\pi$. When $\phi=0$, a symmetric channel with waves out of phase can be described and for $\phi=\pi$, the waves are in phase.

2.2 Modified Darcy-Brinkman model for porous medium

The well-known Darcy law states that, in the flow of a Newtonian fluid through a porous medium, the pressure gradient caused by the friction drag is directly proportional to the velocity. Recently, based on the local volume averaging technique and the balance of forces acting on a volume element of viscoelastic fluids in porous media, Tan and Masuoka[38] developed a modified Darcy-Brinkman model for viscoelastic fluid flows in porous media. Xue and Nie[39] further generalized this model for generalized Maxwell fluid flows in porous media. The Darcy-Brinkman model[40] for generalized Oldroyd-B fluids takes the form:

$$\left(1+\tilde{\lambda}_1^{\alpha}\frac{\partial^{\alpha}}{\partial\tilde{t}^{\alpha}}\right)R = -\frac{\mu\phi}{\tilde{K}}\left(1+\tilde{\lambda}_2^{\beta}\frac{\partial^{\beta}}{\partial\tilde{t}^{\beta}}\right)\tilde{u}, \tag{2}$$

where R, φ, $\tilde{K}$, $\tilde{u}$, μ and $\tilde{\lambda}_1$, $\tilde{\lambda}_2$ designate the Darcy resistance, porosity of porous medium, permeability, axial velocity, viscosity and material constants. α, β are the fractional parameters ($0<\alpha\le\beta\le1$).

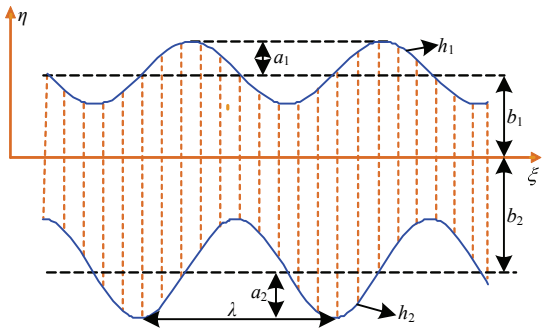

Fig. 1 Geometry of asymmetric porous medium channel.

2.3 Fractional Oldroyd-B model for biofluid

The constitutive equation for fractional Oldroyd-B fluids[40] is given by

$$\left(1+\tilde{\lambda}_1^{\alpha}\frac{\partial^{\alpha}}{\partial\tilde{t}^{\alpha}}\right)\tilde{\tau}=\mu\left(1+\tilde{\lambda}_2^{\beta}\frac{\partial^{\beta}}{\partial\tilde{t}^{\beta}}\right)\dot{\gamma}, \tag{3}$$

where $\tilde{\tau}$, $\dot{\gamma}$ are shear stress and rate of shear strain, respectively.

2.4 Fractional Oldroyd-B model for biofluid

The governing equations of motion for generalized Oldroyd-B fluid[40] through a porous medium are

$$\left.\begin{aligned}\rho\left(\frac{\partial}{\partial\tilde{t}}+\tilde{u}\frac{\partial}{\partial\tilde{\xi}}+\tilde{v}\frac{\partial}{\partial\tilde{\eta}}\right)\tilde{u}&=-\frac{\partial\tilde{p}}{\partial\tilde{\xi}}+\frac{\partial\tilde{\tau}_{\tilde{\xi}\tilde{\xi}}}{\partial\tilde{\xi}}+\frac{\partial\tilde{\tau}_{\tilde{\xi}\tilde{\eta}}}{\partial\tilde{\eta}}+R_{\xi}\\ \rho\left(\frac{\partial}{\partial\tilde{t}}+\tilde{u}\frac{\partial}{\partial\tilde{\xi}}+\tilde{v}\frac{\partial}{\partial\tilde{\eta}}\right)\tilde{v}&=-\frac{\partial\tilde{p}}{\partial\tilde{\eta}}+\frac{\partial\tilde{\tau}_{\tilde{\eta}\tilde{\xi}}}{\partial\tilde{\xi}}+\frac{\partial\tilde{\tau}_{\tilde{\eta}\tilde{\eta}}}{\partial\tilde{\eta}}+R_{\eta}\end{aligned}\right\}, \tag{4}$$

where ρ, $\tilde{v}$, $\tilde{\eta}$, $\tilde{p}$ and R_{ξ}, R_{η} are the fluid density, transverse velocity, transverse coordinate, pressure, and components of Darcy resistance, respectively. We introduce the following non-dimensional parameters

$$\left.\begin{aligned}&\xi=\frac{\tilde{\xi}}{\lambda},\ \ \eta=\frac{\tilde{\eta}}{b_1},\ \ t=\frac{c\tilde{t}}{\lambda},\ \lambda_1=\frac{c\tilde{\lambda}_1}{\lambda},\lambda_2=\frac{c\tilde{\lambda}_2}{\lambda},\\ &h_1=\frac{\tilde{h}_1}{b_1}=1+\phi_1\sin 2\pi(\xi-t),\\ &h_2=\frac{\tilde{h}_2}{b_1}=-b-\phi_2\sin(2\pi(\xi-t)+\phi),\ \phi_1=\frac{a_1}{b_1},\\ &\phi_2=\frac{a_2}{b_1},b=\frac{b_2}{b_1},u=\frac{\tilde{u}}{c},v=\frac{\tilde{v}}{c\delta},p=\frac{\tilde{p}b_1^{\,2}}{\mu c\lambda},\\ &\tau=\frac{b_1\tilde{\tau}}{\mu c},\mathrm{Re}=\frac{\rho c b_1\delta}{\mu},\delta=\frac{b_1}{\lambda},\ K=\frac{\varphi\tilde{K}}{b_1^{\,2}}.\end{aligned}\right\}, \tag{5}$$

where *Re* and *K* are Reynolds number and permeability parameter, respectively. Substituting the values of Darcy resistance and shear stress from Eqs. (2) and (3) into Eq. (4) and using the non-dimensional parameters from Eq. (5), applying the long wavelength and low Reynolds number approximations, Eq. (4) effectively reduces to

$$\left.\begin{aligned}&\left(1+\lambda_1^{\alpha}\frac{\partial^{\alpha}}{\partial t^{\alpha}}\right)\frac{\partial p}{\partial\xi}=\left(1+\lambda_2^{\beta}\frac{\partial^{\beta}}{\partial t^{\beta}}\right)\left(\frac{\partial^2 u}{\partial\eta^2}\right)\\ &-\frac{1}{K}\left(1+\lambda_2^{\beta}\frac{\partial^{\beta}}{\partial t^{\beta}}\right)u,\quad \frac{\partial p}{\partial\eta}=0.\end{aligned}\right\}, \tag{6}$$

The boundary conditions are

$$u=0\ at\ \ \eta=h_1, \tag{7}$$

$$u=0\ at\ \ \eta=h_2, \tag{8}$$

$$\frac{\partial p}{\partial\xi}=p_0\ at\ t=0. \tag{9}$$

2.5 Analysis

Integrating Eq. (6) with respect to η and using Eqs. (7) and (8), the axial velocity is obtained as

$$u=C_1e^{k\eta}+C_2e^{-k\eta}-\frac{1}{k^2}\left(1+\lambda_2^{\beta}\frac{\partial^{\beta}}{\partial t^{\beta}}\right)^{-1}\left(1+\lambda_1^{\alpha}\frac{\partial^{\alpha}}{\partial t^{\alpha}}\right)\frac{\partial p}{\partial\xi}, \tag{10}$$

where $k^2=\frac{1}{K}$,

$$C_1=\frac{1}{k^2}\left(1+\lambda_2^{\beta}\frac{\partial^{\beta}}{\partial t^{\beta}}\right)^{-1}\left(1+\lambda_1^{\alpha}\frac{\partial^{\alpha}}{\partial t^{\alpha}}\right)\frac{\partial p}{\partial\xi}\left(\frac{e^{-kh_2}-e^{-kh_1}}{2\sinh k(h_1-h_2)}\right),$$

$$C_2=\frac{1}{k^2}\left(1+\lambda_2^{\beta}\frac{\partial^{\beta}}{\partial t^{\beta}}\right)^{-1}\left(1+\lambda_1^{\alpha}\frac{\partial^{\alpha}}{\partial t^{\alpha}}\right)\frac{\partial p}{\partial\xi}\left(\frac{e^{kh_2}-e^{kh_1}}{2\sinh k(h_2-h_1)}\right).$$

The volumetric flow rate is defined as

$$Q=\int_{h_2}^{h_1}u\mathrm{d}\eta, \tag{11}$$

which, by virtue of Eq. (10), reduces to Eq. (12).

The transformations between a wave frame $(\tilde{x},\tilde{y})$ moving with velocity *c* and the fixed frame $(\tilde{\xi},\tilde{\eta})$ are given by

$$\tilde{x}=\tilde{\xi}-c\tilde{t},\ \ \tilde{y}=\tilde{\eta},\ \ \tilde{U}=\tilde{u}-c,\ \ \tilde{V}=\tilde{v}, \tag{13}$$

where $(\tilde{U},\tilde{V})$ and $(\tilde{u},\tilde{v})$ are the velocity components in the wave and fixed frame, respectively.

$$Q=\frac{1}{k_2}\left(1+\lambda_2^{\beta}\frac{\partial^{\beta}}{\partial t^{\beta}}\right)^{-1}\left(1+\lambda_1^{\partial}\frac{\partial^{\alpha}}{\partial t^{\alpha}}\right)\frac{\partial p}{\partial\xi}\left(\frac{2\cosh k(h_1-h_2)-2}{k\sinh k(h_1-h_2)}+h_1-h_2\right), \tag{12}$$

The volumetric flow rate in the wave frame is given by

$$q=\int_{h_2}^{h_1} U\mathrm{d}y=\int_{h_2}^{h_1}(u-1)\mathrm{d}\eta\,, \tag{14}$$

which, on integration, yields

$$q=Q+h_2-h_1. \tag{15}$$

Averaging volumetric flow rate along one time period, we get

$$\bar{Q}=\int_0^1 Q\mathrm{d}t=\int_0^1 (q+h_1-h_2)\mathrm{d}t\,, \tag{16}$$

which, on integration, yields

$$\bar{Q}=q+1+b=Q+1+b+h_2-h_1\,, \tag{17}$$

From Eqs. (12) and (17), we obtain

$$\frac{\partial^a}{\partial t^a}\left(\frac{\partial p}{\partial x}\right)+\frac{1}{\lambda_1^a}\frac{\partial p}{\partial x}=\frac{k^2}{\lambda_1^a}\left(1+\lambda_2^\beta\frac{\partial^\beta}{\partial t^\beta}\right)\left(\frac{\bar{Q}-1-b+h_1-h_2}{\dfrac{2\cosh k\left(h_1-h_2\right)-2}{k\sinh k\left(h_1-h_2\right)}+h_2-h_1}\right). \tag{18}$$

3 Solution by differential transform method (DTM)

DTM[36] uses Taylor series expansions to derive differential transforms. Differential transform of boundary conditions is converted into a recurrence equation that finally leads to the solution of a system of algebraic equations. DTM is different from the traditional higher order Taylor series method, the latter requiring symbolic computation and thereby causing greater computational expense for large orders. However, DTM obtains a polynomial series solution by means of an iterative procedure. It is an alternative procedure for obtaining analytic Taylor series solution of differential equations. With this method, it is possible to obtain highly accurate results or exact solutions for differential equations. DTM has a strong advantage in that it can be applied directly to differential equations without requiring linearization, discretization or perturbation. Another important advantage is that this method reduces the size of computational work compared with other approaches. DTM was initially employed in electrical circuit analysis in the mid-1980s. It has re-emerged as a powerful tool in nonlinear mechanics and has demonstrated excellent stability and adaptability for biomedical transport phenomena. In the context of biomechanical engineering, it has been employed to study many complex systems of nonlinear differential equations. Let us consider the following differential equation

$$\frac{\partial^\alpha f(x,t)}{\partial t^\alpha}+\frac{1}{\lambda_1^\alpha}f(x,t)=A+\lambda_2^\beta\frac{\partial^\beta A}{\partial t^\beta}\,, \tag{19}$$

where, $f(x,t)=\dfrac{\partial p}{\partial x}$

and $A=\dfrac{\bar{Q}-1-b+h_1-h_2}{\dfrac{2\cosh k(h_1-h_2)-2}{k\sinh k(h_1-h_2)}+h_2-h_1}$,

with initial condition

$$f(x,0)=0. \tag{20}$$

According to DTM, we can construct the following iteration formula for Eq. (19).

$$\frac{\Gamma(k\alpha+\alpha+1)}{\Gamma(k\alpha+1)}F_{k+1}(x)+\frac{1}{\lambda_1^\alpha}F_k(x)=A\,\delta(k\alpha)+A\lambda_2^\beta\frac{\delta(k\alpha+\beta)}{\Gamma(1-\beta)}$$

$$\text{or}\quad F_{k+1}(x)=\frac{\Gamma(k\alpha+1)}{\Gamma(k\alpha+\alpha+1)}\left[-\frac{1}{\lambda_1^\alpha}F_k(x)+A\,\delta(k\alpha)+A\,\lambda_2^\beta\frac{\delta(k\alpha+\beta)}{\Gamma(1-\beta)}\right], \tag{21}$$

where, $F_{k+1}(x)$ is the DTM of the $f(x,t)$ with respect to t, and $\delta(k)=\begin{cases}1, & k=0\\ 0, & k\neq 0\end{cases}$.

From initial condition Eq. (20), we write

$$F_0(x)=0\,, \tag{22}$$

Substituting Eq. (22) into Eq. (21) and by straightforward iterative steps, we get the following $F_k(x)$ (for $k=0, 1, 2, \ldots, n$) values

$$F_1(x)=\frac{A}{\Gamma(\alpha+1)}\left[1+\lambda_2^\beta\frac{\delta(\beta)}{\Gamma(1-\beta)}\right], \tag{23}$$

$$F_2(x)=\frac{-A}{\lambda_1^{\alpha}\Gamma(2\alpha+1)}\left[1+\lambda_2^{\beta}\frac{\delta(\beta)}{\Gamma(1-\beta)}\right]+A\frac{\Gamma(\alpha+1)}{\Gamma(2\alpha+1)}\left[\delta(\alpha)+\lambda_2^{\beta}\frac{\delta(\alpha+\beta)}{\Gamma(1-\beta)}\right], \tag{24}$$

$$F_3(x)=\frac{A}{\lambda_1^{2\alpha}\Gamma(3\alpha+1)}\left[1+\lambda_2^{\beta}\frac{\delta(\beta)}{\Gamma(1-\beta)}\right]-A\frac{\Gamma(\alpha+1)}{\lambda_1^{\alpha}\Gamma(3\alpha+1)}\left[\delta(\alpha)+\lambda_2^{\beta}\frac{\delta(\alpha+\beta)}{\Gamma(1-\beta)}\right]+A\frac{\Gamma(2\alpha+1)}{\Gamma(3\alpha+1)}\left[\delta(2\alpha)+\lambda_2^{\beta}\frac{\delta(2\alpha+\beta)}{\Gamma(1-\beta)}\right], \tag{25}$$

$$F_4(x)=-\frac{A}{\lambda_1^{3\alpha}\Gamma(4\alpha+1)}\left[1+\lambda_2^{\beta}\frac{\delta(\beta)}{\Gamma(1-\beta)}\right]+A\frac{\Gamma(\alpha+1)}{\lambda_1^{2\alpha}\Gamma(4\alpha+1)}\left[\delta(\alpha)+\lambda_2^{\beta}\frac{\delta(\alpha+\beta)}{\Gamma(1-\beta)}\right]-A\frac{\Gamma(2\alpha+1)}{\lambda_1^{\alpha}\Gamma(4\alpha+1)}\left[\delta(2\alpha)+\lambda_2^{\beta}\frac{\delta(2\alpha+\beta)}{\Gamma(1-\beta)}\right]+A\frac{\Gamma(3\alpha+1)}{\Gamma(4\alpha+1)}\left[\delta(3\alpha)+\lambda_2^{\beta}\frac{\delta(3\alpha+\beta)}{\Gamma(1-\beta)}\right], \tag{26}$$

and so on.

Then the inverse differential transformation of the set of values $F_k(x)$ gives approximate solution as

$$f_n(x,t)=\sum_{k=0}^{n}F_k(x)t^{\frac{k}{\alpha}}, \tag{27}$$

Consequently, the exact solution may be obtained by using

$$f(x,t)=\lim_{n\to\infty}f_n(x,t). \tag{28}$$

The pressure difference across one wavelength (Δp) and friction force across one wavelength at the upper wall (F_1) and the lower wall (F_2) are defined as

$$\Delta p=\int_0^1\frac{\partial p}{\partial x}\mathrm{d}x, \tag{29}$$

$$F_1=\int_0^1 h_1\left(-\frac{\partial p}{\partial x}\right)\mathrm{d}x, \tag{30}$$

$$F_2=\int_0^1 h_2\left(-\frac{\partial p}{\partial x}\right)\mathrm{d}x. \tag{31}$$

4 Numerical results and discussion

We now consider DTM solutions obtained using Mathematica for a range of value of the key dimensionless parameters e.g. fractional parameters, permeability, *etc*. Computations are illustrated in Figs. 2a–2i to Figs. 4a–4i, and in all cases, pressure rise or frictional forces is plotted on the ordinate and averaged volumetric flow rate on the abscissa.

Figs. 2a–2i depict the variation of pressure rise (Δp) with the averaged flow rate $\bar{Q}$ for respectively different values of ratio of upper wall wave amplitude to upper channel half width ($\phi_1=a_1/b_1$), ratio of lower wall wave amplitude to upper channel half width ($\phi_2=a_2/b_1$), lower to upper channel half width ratio ($b=b_2/b_1$), Oldroyd rheological material constants (λ_1, λ_2), fractional viscoelastic parameters (α, β valid for $0<\alpha\leq\beta\leq1$) at fixed dimensionless time (t=0.1). In all these plots, the permeability of the porous medium (K) is high. This corresponds to a sparsely packed porous regime which is representative of weak obstructions present in gastric tracts[3,29,30].

Fig. 2a demonstrates an inverse linear relationship between pressure and averaged flow rate. However pressure rise is clearly elevated with increasing values of ϕ_1 implying that as upper wall wave amplitude is enhanced (or upper channel half width decreased), pressure generated in the peristaltic propulsion is also increased. Physically this implies that stronger peristaltic waves or a constriction in the channel width accentuate pressure rise which will agree with actual observations[2,3] and other mathematical studies such as Yasmin *et al*.[24]. In Fig. 2b, a similar pattern is observed to Fig. 2a, namely the pressure rise is boosted with an increase in ϕ_2 values *i.e*., as lower wall wave amplitude is elevated (or upper channel half width lowered), an escalation is generated in pressure rise in the flow. An increase in phase difference (ϕ) also results in a rise in pressure (Fig. 2c). In all three afore-mentioned plots, the $\bar{Q}$-Δp profiles remain parallel for all values of averaged flow rate $\bar{Q}$ *i.e*., there is no cross-over. Conversely in Fig. 2d, although pressure rise is increased generally with greater values of width ratio ($b=b_2/b_1$) at much higher flow rates, the trend is reversed and thereafter pressure rise is depleted with increasing flow rate and increasing width ratio. Maxi-mum Δp corresponds to zero volumetric flow rate and width ratio. Fig. 2e reveals that with increasing of Oldroyd first material parameter (relaxation time),

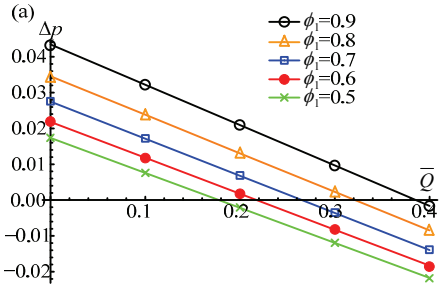

Fig. 2(a) Plot of Δp vs. $\bar{Q}$ for various values of ϕ_1 and b=0.8, ϕ_2=0.5, ϕ=π/2, λ_1=1, λ_2=1, K=1, α=1, β=1, t=0.1.

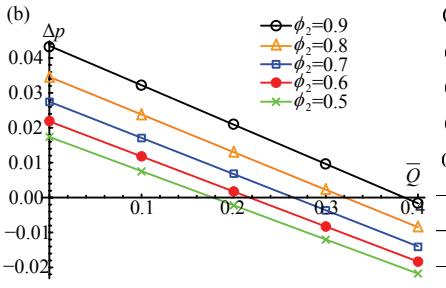

Fig. 2(b) Plot of Δp vs. $\bar{Q}$ for various values of ϕ_2 and b=0.8, ϕ_1=0.5, ϕ=π/2, λ_1=1, λ_2=1, K=1, α=1, β=1, t=0.1.

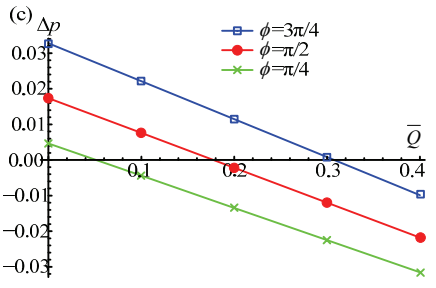

Fig. 2(c) Plot of Δp vs. $\bar{Q}$ for various values of ϕ and b=0.8, ϕ_1=0.5, ϕ_2=0.5, λ_1=1, λ_2=1, K=1, α=1, β=1, t=0.1.

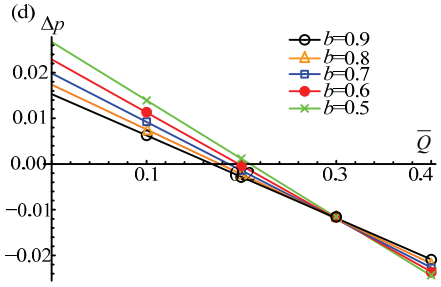

Fig. 2(d) Plot of Δp vs. $\bar{Q}$ for various values of b and ϕ_1=0.5, ϕ_2=0.5, ϕ=π/2, λ_1=1, λ_2=1, K=1, α=1, β=1, t=0.1.

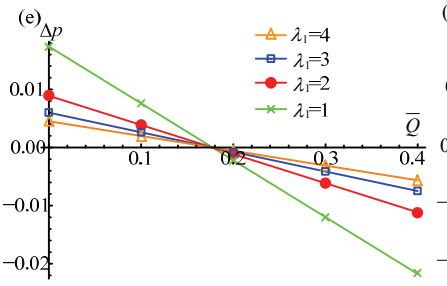

Fig. 2(e) Plot of Δp vs. $\bar{Q}$ for various values of λ_1 and b=0.8, ϕ_1=0.5, ϕ_2=0.5, ϕ=π/2, λ_2=1, K=1, α=1, β=1, t=0.1.

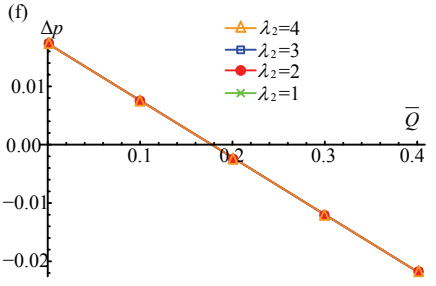

Fig. 2(f) Plot of Δp vs. $\bar{Q}$ for various values of λ_2 and b=0.8, ϕ_1=0.5, ϕ_2=0.5, ϕ=π/2, λ_1=1, K=1, α=1, β=1, t=0.1.

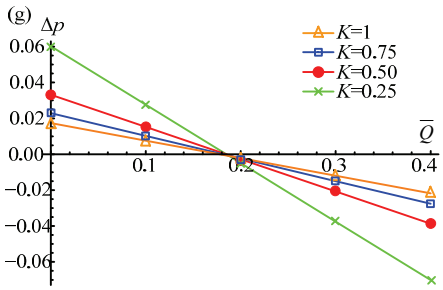

Fig. 2(g) Plot of Δp vs. $\bar{Q}$ for various values of K and b=0.8, ϕ_1=0.5, ϕ_2=0.5, ϕ=π/2, λ_1=1, λ_2=1, α=1, β=1, t=0.1.

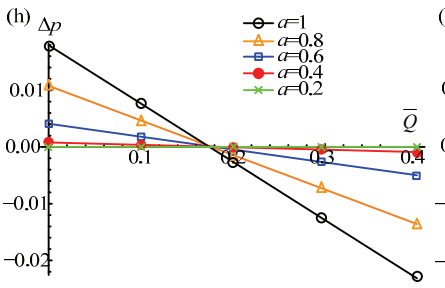

Fig. 2(h) Plot of Δp vs. $\bar{Q}$ for various values of α and b=0.8, ϕ_1=0.5, ϕ_2=0.5, ϕ=π/2, λ_1=1, λ_2=1, K=1, β=1, t=0.1.

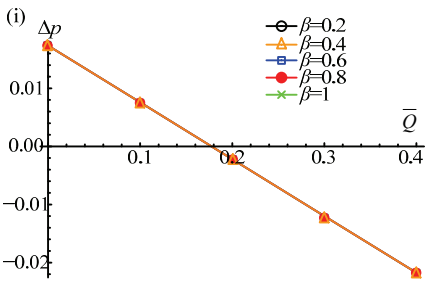

Fig. 2(i) Plot of Δp vs. $\bar{Q}$ for various values of β and b=0.8, ϕ_1=0.5, ϕ_2=0.5, ϕ=π/2, λ_1=1, λ_2=1, K=1, α=1, t=0.1.

difference magnitudes are boosted at higher flow rates; however when a critical flow rate is attained, the contrary behavior is witnessed. Evidently the rheology as reflected in the material parameter, λ_1, exerts a non-negligible influence on pressure-flow response. On the other hand, Fig. 2f demonstrates that a strong increase in the second Oldroyd material parameter, λ_2, generates no tangible modification in pressure rise-flow rate profile. Fig. 2g shows that the effect of decreasing permeability in the regime is to significantly elevate pressure rise in the channel, at low volumetric flow rates. This is attributable to the corresponding increase in obstructions present in the channel as K decreases. Lower permeability implies a greater concentration of debris in the gastric tract and vice versa for higher permeability. In the absolute limit of infinite K, all solid particles vanish and the regime is purely fluid. A very different response however is computed at higher volumetric flow rates. For this scenario, increasing permeability serves to infact depress pressure rise in the regime. Figs. 2h and 2i illustrate the pressure-flow rate profiles for various values of the first and second fractional parameters, α and β. Greater values of α significantly boost pressure rise for lower volumetric flow rates, whereas

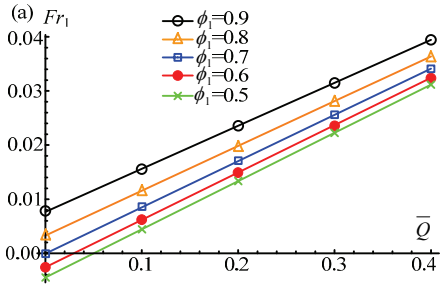

Fig. 3(a) Plot of Fr_1 vs. $\bar{Q}$ for various values of ϕ_1 and b=0.8, ϕ_2=0.5, ϕ=π/2, λ_1=1, λ_2=1, K=1, α=1, β=1, t=0.1.

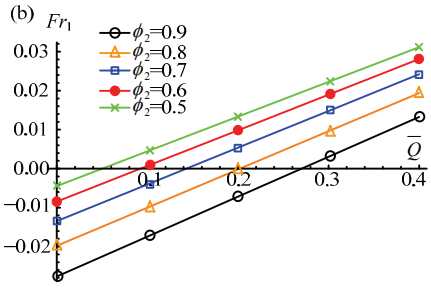

Fig. 3(b) Plot of Fr_1 vs. $\bar{Q}$ for various values of ϕ_2 and b=0.8, ϕ_1=0.5, ϕ=π/2, λ_1=1, λ_2=1, K=1, α=1, β=1, t=0.1.

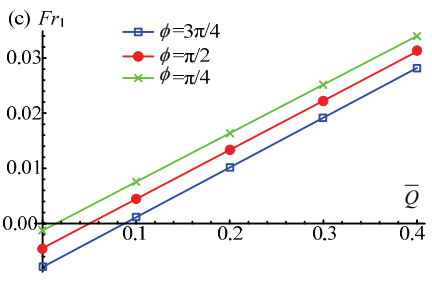

Fig. 3(c) Plot of Fr_1 vs. $\bar{Q}$ for various values of ϕ and b=0.8, ϕ_1=0.5, ϕ_2=0.5, λ_1=1, λ_2=1, K=1, α=1, β=1, t=0.1.

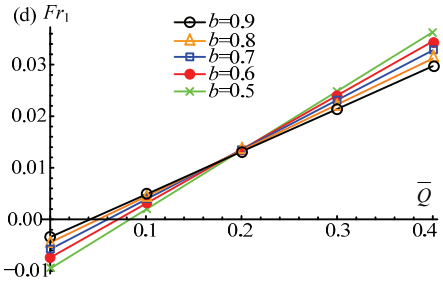

Fig. 3(d) Plot of Fr_1 vs. $\bar{Q}$ for various values of b and ϕ_1=0.5, ϕ_2=0.5, ϕ=π/2, λ_1=1, λ_2=1, K=1, α=1, β=1, t=0.1.

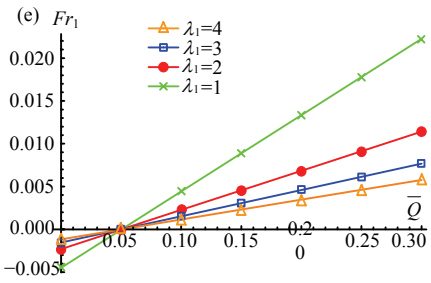

Fig. 3(e) Plot of Fr_1 vs. $\bar{Q}$ for various values of λ_1 and b=0.8, ϕ_1=0.5, ϕ_2=0.5, ϕ=π/2, λ_2=1, K=1, α=1, β=1, t=0.1.

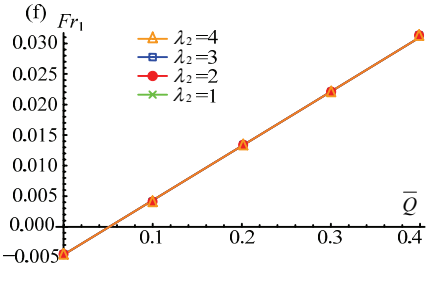

Fig. 3(f) Plot of Fr_1 vs. $\bar{Q}$ for various values of λ_2 and b=0.8, ϕ_1=0.5, ϕ_2=0.5, ϕ=π/2, λ_1=1, K=1, α=1, β=1, t=0.1.

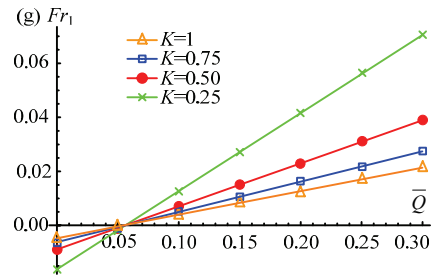

Fig. 3(g) Plot of Fr_1 vs. $\bar{Q}$ for various values of K and b=0.8, ϕ_1=0.5, ϕ_2=0.5, ϕ=π/2, λ_1=1, λ_2=1, α=1, β=1, t=0.1.

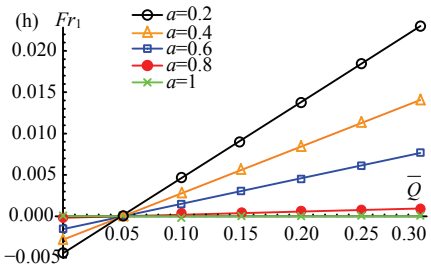

Fig. 3(h) Plot of Fr_1 vs. $\bar{Q}$ for various values of α and b=0.8, ϕ_1=0.5, ϕ_2=0.5, ϕ=π/2, λ_1=1, λ_2=1, K=1, β=1, t=0.1.

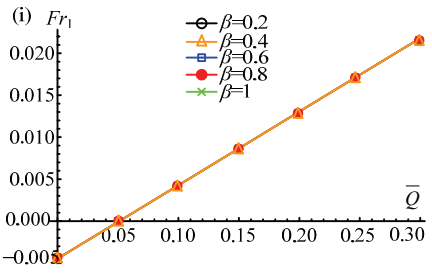

Fig. 3(i) Plot of Fr_1 vs. $\bar{Q}$ for various values of β and b=0.8, ϕ_1=0.5, ϕ_2=0.5, ϕ=π/2, λ_1=1, λ_2=1, K=1, α=1, t=0.1.

the converse response is apparent at higher flow rates. Clearly however increasing values of second fractional parameter β, does not affect the $\bar{Q}$-Δp distributions. In this case the same pressure rise values occur for all flow rates and they are maximized at zero flow rate.

Figs. 3a–3i depict the distributions of upper channel wall friction force (shearing force) (Fr_1) with the averaged flow rate $\bar{Q}$ again for respectively different values of ratio of upper wall wave amplitude to upper channel half width ($\phi_1=a_1/b_1$), ratio of lower wall wave amplitude to upper channel half width ($\phi_2=a_2/b_1$), lower to upper channel half width ratio ($b= b_2/b_1$), Oldroyd rheological material constants (λ_1, λ_2), fractional viscoelastic parameters (α, β valid for $0<\alpha\leq\beta\leq1$) also at t=0.1. In all the graphs, there is a generic rise in friction force, (Fr_1) with increasing volumetric flow rate. The relationship is also linear. Fig. 3a shows that Fr_1 is strongly increased with increasing values of ϕ_1 Higher upper wall wave amplitude is clearly assistive to the rate of propulsion in the channel which accelerates flow and boosts the shearing force on the upper wall. In Fig. 3b, the reverse response is computed and friction force is observed to diminish with an increase in ϕ_2 values, *i.e.*, as lower wall wave amplitude is elevated (or upper

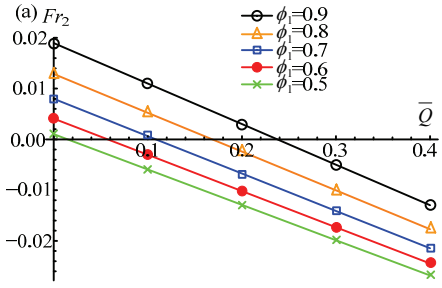

Fig. 4(a) Plot of Fr_2 vs. $\bar{Q}$ for various values of ϕ_1 and b=0.8, ϕ_2=0.5, ϕ=π/2, λ_1=1, λ_2=1, K=1, α=1, β=1, t=0.1.

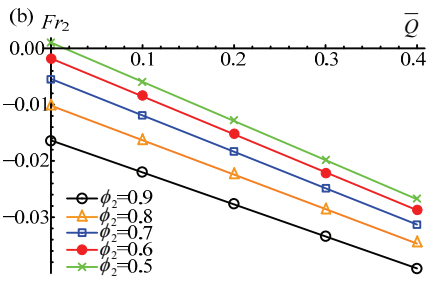

Fig. 4(b) Plot of Fr_2 vs. $\bar{Q}$ for various values of ϕ_2 and b=0.8, ϕ_1=0.5, ϕ=π/2, λ_1=1, λ_2=1, K=1, α=1, β=1, t=0.1.

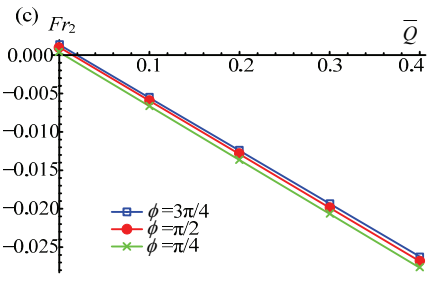

Fig. 4(c) Plot of Fr_2 vs. $\bar{Q}$ for various values of ϕ and b=0.8, ϕ_1=0.5, ϕ_2=0.5, λ_1=1, λ_2=1, K=1, α=1, β=1, t=0.1.

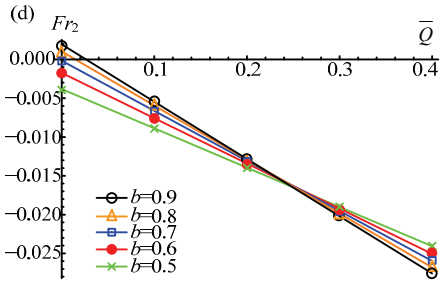

Fig. 4(d) Plot of Fr_2 vs. $\bar{Q}$ for various values of b and ϕ_1=0.5, ϕ_2=0.5, ϕ=π/2, λ_1=1, λ_2=1, K=1, α=1, β=1, t=0.1.

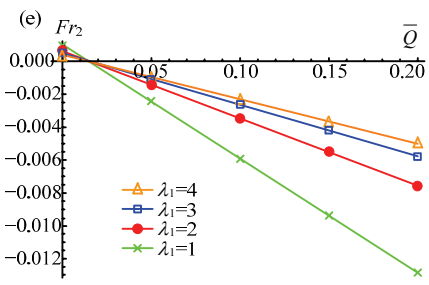

Fig. 4(e) Plot of Fr_2 vs. $\bar{Q}$ for various values of λ_1 and b=0.8, ϕ_1=0.5, ϕ_2=0.5, ϕ=π/2, λ_2=1, K=1, α=1, β=1, t=0.1.

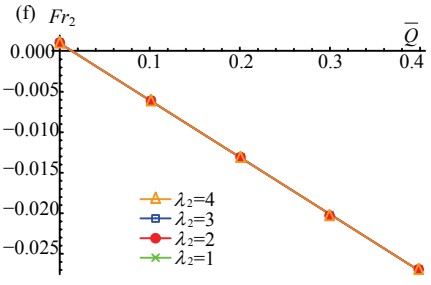

Fig. 4(f) Plot of Fr_2 vs. $\bar{Q}$ for various values of λ_2 and b=0.8, ϕ_1=0.5, ϕ_2=0.5, ϕ=π/2, λ_1=1, K=1, α=1, β=1, t=0.1.

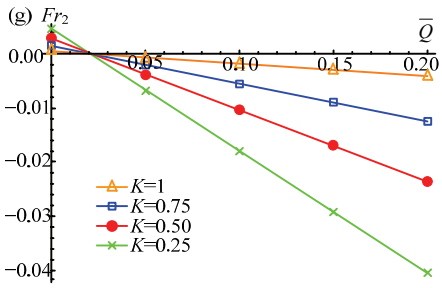

Fig. 4(g) Plot of Fr_2 vs. $\bar{Q}$ for various values of K and b=0.8, ϕ_1=0.5, ϕ_2=0.5, ϕ=π/2, λ_1=1, λ_2=1, α=1, β=1, t=0.1.

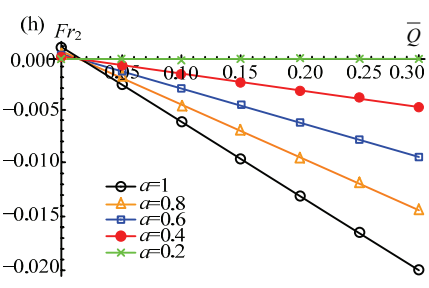

Fig. 4(h) Plot of Fr_2 vs. $\bar{Q}$ for various values of α and b=0.8, ϕ_1=0.5, ϕ_2=0.5, ϕ=π/2, λ_1=1, λ_2=1, K=1, β=1, t=0.1.

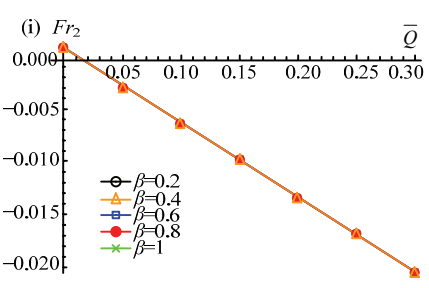

Fig. 4(i) Plot of Fr_2 vs. $\bar{Q}$ for various values of β and b=0.8, ϕ_1=0.5, ϕ_2=0.5, ϕ=π/2, λ_1=1, λ_2=1, K=1, α=1, t=0.1.

channel half width lowered) the upper wall shearing force is reduced. Fig. 3c shows that an increase in phase difference (ϕ) markedly depletes the friction force Fr_1. In Figs. 3a–3c the $\bar{Q}$-Δp profiles are sustained as parallel to each other for all values of averaged flow rate $\bar{Q}$, *i.e.*, there is no cross-over. However in Fig. 3d, although friction force is enhanced with larger values of width ratio (b= b_2/b_1), after a critical flow rate (approximately 0.2), the opposite effect is observed and friction force is seen to be depressed with increasing flow rate and increasing width ratio. Fig. 3e shows that as Oldroyd first material parameter, λ_1, is increased, for lower flow rates, upper wall friction force values are initially decreased; however beyond a critical flow rate is attained, the response is reversed. Overall a strong influence on friction force is associated with the material parameter, λ_1. Conversely Fig. 3f shows that despite a large elevation in the second Oldroyd material parameter, λ_2 the upper wall friction force is unaffected at any flow rate. Inspection of Fig. 3g demonstrates that generally (except for very low flow rates), an increase in permeability parameter, K, serves to markedly enhance upper wall friction force. With increasing permeability, the peristaltic flow receives less impedance from obstructions and is acceler-

ated, manifesting in a greater shearing at the upper wall, *i.e.*, higher friction forces. Figs. 3h and 3i show respectively that with higher values of first fractional parameter, α (except for extremely low flow rates), the upper wall friction force is depressed significantly, whereas with any change in second fractional parameter, β, the friction force profiles remain unaltered.

Figs. 4a–4i present the profiles of lower channel wall friction force (shearing force) (Fr_2) with the averaged flow rate $\bar{Q}$ again for respectively different values of ratio of upper wall wave amplitude to upper channel half width ($\phi_1=a_1/b_1$), ratio of lower wall wave amplitude to upper channel half width ($\phi_2=a_2/b_1$), lower to upper channel half width ratio ($b= b_2/b_1$), relaxation and retardation time constants (λ_1, λ_2), fractional viscoelastic parameters (α, β valid for $0<\alpha\leq\beta\leq1$) also at $t = 0.1$. In all the graphs, there is an overall decrease in friction force (Fr_2) with increasing volumetric flow rate ($\bar{Q}$). The relationship although linear is the opposite of that observed in Figs. 3a–3i for the upper wall friction force, Fr_1. Fr_2 (Fig. 4a) is strongly increased with increasing values of ϕ_1 However in Fig. 4b, the opposite effect is seen and lower wall friction force decreases with an increase in ϕ_2 values. Fig. 4c demonstrates that rising phase difference (ϕ) weakly enhances the friction force Fr_2 In Figs. 4a–4c the $\bar{Q}$-Δp plots remain parallel to each other for all values of averaged flow rate $\bar{Q}$ *i.e.*, there is no cross-over, as observed earlier in Figs. 2a–2c and Figs. 3a–3c. However in Fig. 4d, despite an initial rise in lower wall friction force with greater width ratio ($b= b_2/b_1$), at higher flow rates, the friction force is lowered with increasing flow rate and increasing width ratio. Fig. 4e shows that as relaxation time, λ_1, is increased at lower flow rates, lower wall friction force values are slightly enhanced whereas subsequently beyond a critical flow rate, they are massively reduced. The effect of the material parameter, λ_1 on lower friction force is strong. Conversely in Fig. 4f, the second Oldroyd material parameter, λ_2 (retardation time) has no effect on lower friction force. From inspection of Fig. 4g, it is apparent that generally (except for very low flow rates), an increase in permeability parameter, K, serves to markedly elevate the lower wall friction force, and this is as described earlier a result of peristaltic flow acceleration with greater permeability. Figs. 4h–4i show respectively that with greater first fractional parameter, α (except for extremely low flow rates), the lower wall friction force is strongly lowered, whereas with any modification in second fractional parameter, β, the friction force profiles are as with pressure rise (Fig. 2i) or upper wall friction force (Fig. 3i) not affected.

5 Conclusion

A theoretical and numerical study of peristaltic flow of non-Newtonian biofluids in a two-dimensional asymmetric channel containing porous media has been presented, motivated by modelling obstructed digestive (intestinal) transport. The fractional viscoelastic Oldroyd-B rheological model has been employed to simulate biorheological characteristics and a modified Darcy-Brinkman model for the effect of the porous media impedance. The differential transform method (DTM), a semi-numerical technique has been utilized to derive approximate analytical solutions to the boundary value problem. Mathematica software is employed to evaluate solutions for various parametric effects *i.e.*, fractional (rheological material) parameters, relaxation time, retardation time, amplitude of the wave, and permeability parameter on peristaltic flow characteristics such as volumetric flow rate, pressure difference and wall friction force. The present model is relevant to flow in diseased intestines. DTM computations have shown that with increasing Oldroyd first material parameter (relaxation time), pressure difference magnitudes and upper and lower wall friction force are strongly influenced whereas they are not affected with second Oldroyd material parameter (retardation time). Also except for very low flow rates, larger permeability parameter has been shown to strongly elevate upper and lower wall friction force, owing to an accelerating effect on the peristaltic propulsion regime, respectively. The first fractional parameter is also found to have a major influence on pressure rise and friction forces whereas the second fractional parameter exerts no discernible effects. Other interesting flow characteristics have been revealed of relevance to diseased gastric transport. The present study should serve to provide a good benchmark for further investigations into intestinal propulsion flows with obstructions. A major endeavor is underway to utilize commercial CFD codes e.g. ADINA-F to simulate such problems in three dimensions with more sophisticated and realistic geometrical characteristics. The

results of such investigations will be communicated imminently.

References

[1] Elman R. The danger of sudden deflation of acutely distended bowel in late low intestinal obstruction. *The American Journal of Surgery*, 1934, **26**, 438–446.

[2] Grassi R, Romano S, D'Amario F, Giorgio Rossi A, Romano L, Pinto F, Di Mizio R. The relevance of free fluid between intestinal loops detected by sonography in the clinical assessment of small bowel obstruction in adults. *European Journal of Radiology*, 2004, **50**, 5–14.

[3] Farrell J J. Methods in Disease: Investigating the Gastrointestinal Tract. *Gastroenterology*, 1999, **116**, 1009–1010.

[4] Rommel N, Selleslagh M, Rosen R L, L Rodriguez, Kritas S, Scheerens C, Tack J F, Omari T, Nurko S. Esophageal pressure topography (ept) incorporating pressure flow analysis discriminates dysphagia due to weak peristalsis from dysphagia due to abnormal bolus flow resistance in children. *Gastroenterology*, 2013, **144**, S170–S170.

[5] Kishi K, Yamada K. Sugiyama T. Gastric outlet obstruction caused by a large gallstone in the duodenum (Bouveret's syndrome). *Clinical Gastroenterology and Hepatology*, 2008, **6**, e11.

[6] Bég O A, Uddin M J, Khan W A. Bioconvective non-Newtonian nanofluid transport in porous media containing micro-organisms in a moving free stream. *Journal of Mechanics Medicine Biology*, 2015, **15**, 1550071.

[7] Sukop M C, Van Dijk G J, Perfect E, Van Loon W K P. Percolation thresholds in 2-dimensional prefractal models of porous media. *Transport in Porous Media*, 2002, **48**, 187–208.

[8] Frangi, A F, Lassila T, Vardakis J C, Ventikos Y. Multiscale modelling of transport phenomena in biological tissue. *4th International Conference on Computational and Mathematical Biomedical Engineering (CMBE*2015*)*, France, 2015.

[9] Zidi M, Tounsi A, Houari M S A, Bedia A A, Bég O A. Bending analysis of FGM plates under hgro-thermo-mechanical loading using a four variable refined plate theory. *Aerospace Science and Technology*, 2014, **34**, 24–34.

[10] Rohan E. Modeling Large-deformation-induced microflow in soft biological tissues. *Theoretical and Computational Fluid Dynamics*, 2006, **20**, 251–276.

[11] Kothandapani M, Srinivas S. Non-linear peristaltic transport of a Newtonian fluid in an inclined asymmetric channel through a porous medium. *Physics Letters A*, 2008, **372**, 1265–1276.

[12] Mekheimer K S, Abd Elmaboud Y. Peristaltic flow through a porous medium in an annulus: Application of an endoscope. *Applied Mathematics & Information Sciences*, 2008, **2**, 103–121.

[13] El Shehawey F, Husseny S Z A. Effects of porous boundaries on peristaltic transport through a porous medium. *Acta Mechanica*, 2000, **143**, 165–177.

[14] Mekheimer K S. Non-linear peristaltic transport through a porous medium in an inclined planar channel. *Journal of Porous Media*, 2003, **6**, 189–201.

[15] Srinivas S, Gayathri R. Peristaltic transport of a Newtonian fluid in a vertical asymmetric channel with heat transfer and porous medium. *Applied Mathematics and Computation*, 2009, **215**, 185–196.

[16] Skalak R, Ozkaya N, Skalak T C. Biofluid Mechanics. *Annual Review of Fluid Mechanics*, 1989, **21**, 167–200.

[17] Radhakrishnamacharya G. Long wave length approximation to peristaltic motion of a power-law fluid. *Rheologica Acta*, 1982, **21**, 30–35.

[18] Li W G, Luo X Y, Chin S B, Hill N A, Johnson A G, Bird N C. Non-Newtonian bile flow in elastic cystic duct: One- and three-dimensional modeling. *Annals of Biomedical Engineering*, 2008, **36**, 1893–1908.

[19] Akbar N S, Nadeem S. Simulation of peristaltic flow of chyme in small intestine for couple stress fluid. *Meccanica*, 2013, **49**, 325–334.

[20] Muthu P, Ratish Kumar B V, Chandra P. Peristaltic motion of micropolar fluid in circular cylindrical tubes: Effect of wall properties. *Applied Mathematical Modelling*, 2008, **32**, 2019–2033.

[21] Vicente J D. *Viscoelasticity – From Theory to Biological Applications*, InTech, Virginia, USA, 2012.

[22] Norouzi M, Davoodi M, Bég O A, Joneidi A A. Analysis of the effect of normal stress differences on heat transfer in creeping viscoelastic Dean flow. *International Journal of Thermal Sciences,* 2013, **69**, 61–69.

[23] Tripathi D. Numerical and analytical simulation of peristaltic flows of generalized Oldroyd-B fluids. *International Journal for Numerical Methods in Fluids*, 2011, **67**, 1932–1943.

[24] Yasmin H, Hayat T, Alsaedi A, Alsulami H H. Peristaltic flow of Johnson-Segalman fluid in asymmetric channel with convective boundary conditions. *Applied Mathematics and Mechanics*, 2014, **35**, 697–716.

[25] Tripathi D, Pandey S K, Bég O A. Mathematical modelling of heat transfer effects on swallowing dynamics of viscoelastic flood bolus through the human oesophagus. *Interna-*

tional Journal of Thermal Sciences, 2013, **70**, 41–53.

[26] Tripathi D, Bég O A, Curiel-Sosa J L. Homotopy Semi-Numerical Simulation of Peristaltic flow of generalized Oldroyd-B fluids with slip effects. *Computer Methods in Biomechanics and Biomedical Engineering*, 2014, **17**, 433–442.

[27] Alemayehu H, Radhakrishnamacharya G. The dispersion in peristaltic flow of micropolar fluid in a porous medium. *Journal of Porous Media*, 2012, **15**, 1067–1077.

[28] Mekheimer K S. Non-linear peristaltic transport of a second-order fluid through a porous medium. *Applied Mathematical Modelling*, 2010, **35**, 2695–2710.

[29] Tripathi D, Bég O A. A numerical study of oscillating peristaltic flow of generalized Maxwell viscoelastic fluids through a porous medium. *Transport in Porous Media*, 2012, **95**, 337–348.

[30] Alemayehu H, Radhakrishnamacharya G. Dispersion of a solute in peristaltic motion of a couple stress fluid through a porous medium. *Tamkang Journal of Mathematics*, 2012, **43**, 541–555.

[31] Tripathi D. Peristaltic hemodynamic flow of couple-stress fluids through a porous medium with slip effect. *Transport in Porous Media*, 2012, **92**, 559–572.

[32] Oldroyd J G. On the formulation of rheological equations of state. *Proceedings of the Royal Society of London A*, 1950, **200**, 523–541.

[33] Qi H, Xu M. Some unsteady unidirectional flows of a generalized Oldroyd-B fluid with fractional derivative. *Applied Mathematical Modelling*, 2009, **33**, 4184–4191.

[34] Nadeem S. General periodic flows of fractional Oldroyd-B fluid for an edge. *Physics Letters A*, 2007, **368**, 181–187.

[35] Liu Y, Zheng L, Zhang X. Unsteady MHD Couette flow of a generalized Oldroyd-B fluid with fractional derivative. *Computers and Mathematics with Applications*, 2011, **61**, 443–450.

[36] Zhou J K. *Differential Transformation and its Application for Electrical Circuits*, Huazhong University Press, Wuhan, 1986.

[37] Rashidi M M, Parsa A B, Bég O A, Shamekhi L, Sadri S M, Bég T A. Parametric analysis of entropy generation in magneto-hemodynamic flow in a semi-porous channel with OHAM and DTM. *Applied Bionics and Biomechanics*, 2014, **11**, 1–2.

[38] Tan W C, Masuoka T. Stokes' first problem for an Oldroyd-B fluid in a porous half space. *Physics of Fluids*, 2005, **17**, 023101.

[39] Xue C, Nie J. Exact solutions of Rayleigh-Stokes problem for heated generalized Maxwell fluid in a porous half-space. *Mathematical Problems in Engineering*, 2008, **2008**, 641431.

[40] Khan M, Hayat T, Asghar S. Exact solution for MHD flow of a generalized Oldroyd-B fluid with modified Darcy's law. *International Journal of Engineering Sciences*, 2006, **44**, 333–339.

Appendix-1

The DTM computational algorithm is validated using well known He's homotopy perturbation method (HPM). Consider the equation

$$\frac{\partial^\alpha f}{\partial t^\alpha}+\frac{1}{\lambda_1^\alpha} f = A+\lambda_2^\beta \frac{\partial^\beta}{\partial t^\beta}(A),\ 0<\alpha\le 1, \qquad \text{(A1)}$$

with initial condition

$$f(x,0)=0. \qquad \text{(A2)}$$

According to the HPM, we construct the following homotopy

$$\frac{\partial^\alpha f}{\partial t^\alpha}=\bar{h}\left[-\frac{1}{\lambda_1^\alpha} f + A+\lambda_2^\beta \frac{\partial^\beta}{\partial t^\beta}(A)\right], \qquad \text{(A3)}$$

where the homotopy parameter $\bar{h}$ is considered as a small parameter ($\bar{h}\in[0,1]$). Now applying the classical perturbation technique, we can assume that the solution of Eq. (A1) can be expressed as a power series in p as given below

$$f=f_0+\bar{h}f_1+\bar{h}^2 f_2+\bar{h}^3 f_3+\bar{h}^4 f_4+\cdots, \qquad \text{(A4)}$$

when $\bar{h} \to 1$, Eq. (A3) corresponds to Eq. (A1) and Eq. (A4) becomes the approximate solution of Eq. (A1). Substituting Eq. (A4) in Eq. (A3) and comparing the like powers of $\bar{h}$, we obtain the following set of linear differential equations

$$\bar{h}^0 : \; D_t^a f_0 = 0, \tag{A5}$$

$$\bar{h}^1 : \; D_t^a f_1 = -\frac{1}{\lambda_1^\alpha} f_0 + A + \lambda_2^\beta \frac{\partial^\beta}{\partial t^\beta}(A), \tag{A6}$$

$$\bar{h}^2 : \; D_t^a f_2 = -\frac{1}{\lambda_1^\alpha} f_1, \tag{A7}$$

$$\bar{h}^3 : \; D_t^a f_3 = -\frac{1}{\lambda_1^\alpha} f_2, \tag{A8}$$

$$\bar{h}^4 : \; D_t^a f_4 = -\frac{1}{\lambda_1^\alpha} f_3, \tag{A9}$$

and so on.

The method is based on applying the operator J_t^a (the inverse operator of Caputo derivative D_t^a) on both sides of the Eqs. (A5–A9), then we obtain the components f_n, n≥0.

Finally, we approximate the analytical solution $f(x,t)$ by the truncated series:

$$f(x,t) = \lim_{N\to\infty} \Phi_N(x,t), \tag{A10}$$

where:

$$\Phi_N(x,t) = \sum_{n=0}^{N-1} f_n(x,t). \tag{A11}$$

The above series solutions generally converge very rapidly. A classical approach of convergence of this type of series is already presented in literature.

Table 1 Comparison table of DTM and HPM results of Δp for various values of ϕ_1 and $\bar{Q}$ and b=0.8, ϕ_2=0.5, ϕ=π/2, λ_1=1, λ_2=1, K=1, α=1, β=1, t=1

	$\bar{Q}$=0.1		$\bar{Q}$=0.3	
	Δp_{DTM}	Δp_{HPM}	Δp_{DTM}	Δp_{HPM}
ϕ_1=0.5	0.095120425	0.095138017	0.017230189	0.017241089
ϕ_1=0.6	0.137151649	0.137180157	0.050937477	0.050901749
ϕ_1=0.7	0.197820059	0.197800173	0.099989816	0.099918943
ϕ_1=0.8	0.286952040	0.286981045	0.172686734	0.172616284
ϕ_1=0.9	0.421794668	0.421800179	0.283663418	0.283601837

Table 2 Comparison table of DTM and HPM results of Δp for various values of ϕ_2 and $\bar{Q}$ and b=0.8, ϕ_1=0.5, ϕ=π/2, λ_1=1, λ_2=1, K=1, α=1, β=1, t=1

	$\bar{Q}$=0.1		$\bar{Q}$=0.3	
	Δp_{DTM}	Δp_{HPM}	Δp_{DTM}	Δp_{HPM}
ϕ_2=0.5	0.056175307	0.056538905	−0.021714927	−0.021920528
ϕ_2=0.6	0.094044563	0.094105739	0.007830390	0.007739266
ϕ_2=0.7	0.148904937	0.148038278	0.051074694	0.051295380
ϕ_2=0.8	0.229819387	0.229245290	0.115554081	0.115648438
ϕ_2=0.9	0.352729043	0.352629403	0.214597793	0.214385630